Magnetic properties of honeycomb-based spin models in verdazyl-based salts

S. Miyamoto, Y. Iwasaki, N. Uemoto, Y. Hosokoshi, H. Fujiwara, S. Shimono, and H. Yamaguchi[*]

Department of Physical Science, Osaka Prefecture University, Osaka 599-8531, Japan

We successfully synthesized the verdazyl-based salts $(m\text{-MePy-V})_2\text{Fe}_2\text{OCl}_6$ and $[m\text{-MePy-V} -(p\text{-Cl})_2]_2\text{Fe}_2\text{OCl}_6 \cdot (\text{CH}_3\text{CN})_2$ with different $\text{Fe}_2\text{OCl}_6^{2-}$ structures. The exchange interactions between Fe^{3+} ions in the $\text{Fe}_2\text{OCl}_6^{2-}$ anions were evaluated to be nearly equivalent and to form an $S = 5/2$ antiferromagnetic (AF) dimer in each salt. We obtained the magnetic susceptibility of $S = 1/2$ spins on the radical by subtracting the contribution of $S = 5/2$ spins in the anion from the observed magnetic susceptibility. For $(m\text{-MePy-V})_2\text{Fe}_2\text{OCl}_6$, *ab initio* molecular orbital (MO) calculations indicated that the $S = 1/2$ AF dimers are weakly connected by ferromagnetic interactions, thereby forming a honeycomb lattice. The experimentally measured magnetic susceptibility and specific heat indicate a corresponding nonmagnetic gapped behavior. For $[m\text{-MePy-V}-(p\text{-Cl})_2]_2\text{Fe}_2\text{OCl}_6 \cdot (\text{CH}_3\text{CN})_2$, MO calculations indicated that four types of dominant interactions form an unconventional $S = 1/2$ honeycomb-based 3D spin model. The magnetic susceptibility and specific heat indicate a phase transition to a 3D order at approximately 4.8 K.

I. INTRODUCTION

Honeycomb structures in condensed-matter systems are an attractive subject owing to unique physical properties. The most widely known example, graphene, is composed of carbon atoms arranged in a honeycomb structure, and its unusual electronic excitations, called Dirac electrons, induce unconventional phenomena [1–3]. Recent studies on the Kitaev model have further promoted interest in honeycomb lattices. This exactly solvable quantum spin model is composed of $S = 1/2$ spins coupled by bond-dependent Ising interactions on a honeycomb lattice, and its ground state has been shown to be a quantum spin liquid with excitations associated with Majorana fermions [4–6]. In the case of an $S = 1/2$ Heisenberg antiferromagnetic (HAF) honeycomb lattice, which is the basic spin model for a honeycomb structure, the ground state is known to be a Néel order. However, its magnetic moments per site are largely reduced by quantum fluctuations owing to the relatively small coordination number [7–10]. Because the ordered state of an $S = 1/2$ HAF honeycomb lattice is fragile owing to its quantum fluctuations, a relatively small lattice distortion can induce a disordered phase. A dimerlike distortion, which corresponds to the honeycomb-based spin models in the present paper, is numerically studied [11,12]. It is predicted that a dimerlike distortion causes a quantum phase transition (QPT) from the Néel order phase to a gapped dimer phase at a critical distortion ratio. The evaluated quantum critical exponents indicate that the quantum criticality falls in the $O(3)$ universality class. In the gapped dimer phase, the spin gap is closed by applying a magnetic field, and a field-induced QPT appears at a critical field. The magnetization curve exhibits almost linear behavior in the vicinity of the field-induced QPT, which reflects the two-dimensionality of the distorted honeycomb lattice and is clearly different from

square-root behavior in gapped 1D spin systems. Because a field-induced QPT in real 2D spin systems induces the Bose-Einstein condensation (BEC) of magnons, the distorted honeycomb lattice can be a very effective model for the investigation of transport properties in a magnon BEC on a honeycomb lattice. However, in inorganic compounds, there are only a few model substances for the $S = 1/2$ HAF honeycomb lattice [13–15]

We have been developing material designs for quantum spin systems using verdazyl radicals. Our previous works realized a variety of unconventional spin systems, including ferromagnetic-leg ladders, quantum pentagons, and random singlets, that had not been realized in the field of conventional inorganic materials [16–20]. The formation of $S = 1/2$ HAF honeycomb lattices with ordered ground states was confirmed in several compounds [21,22]. As a next step in material design, we have been developing the synthesis of verdazyl-based salts by combining cationized verdazyl radicals with anions. By reflecting the structural characteristics of various kinds of anions in the synthesized salts, we are progressing toward realizing more attractive quantum spin models than those that have been realized so far [23,24].

In this paper, we present verdazyl-based charge-transfer salts forming spin lattices based on a distorted honeycomb lattice. We successfully synthesized single crystals of $(m\text{-MePy-V})_2\text{Fe}_2\text{OCl}_6$ [$m\text{-MePy-V}$ = 3-(3-methylpyridyl)-1,5-diphenylverdazyl] and $[m\text{-MePy-V}-(p\text{-Cl})_2]_2\text{Fe}_2\text{OCl}_6 \cdot (\text{CH}_3\text{CN})_2$ [$m\text{-MePy-V}-(p\text{-Cl})_2$ = 3-(3-methylpyridyl)-1,5-bis(4-chlorophenyl)-verdazyl]. The exchange interaction between Fe^{3+} ions in the $\text{Fe}_2\text{OCl}_6^{2-}$ anion forms an $S = 5/2$ AF dimer in each salt. We obtained the magnetic susceptibility of $S = 1/2$ on the radicals by subtracting the contribution of the $S = 5/2$ dimers in the anion from the observed magnetic susceptibility. For the former salt, *ab initio* molecular orbital (MO) calculations indicate that the $S = 1/2$ AF dimers are weakly connected by ferromagnetic interactions, thereby forming a honeycomb lattice. For the latter salt, MO

calculations indicate that four types of dominant interactions form an unconventional $S = 1/2$ honeycomb-based 3D spin model.

II. EXPERIMENTAL

We synthesized *m*-MePy-V and *m*-MePy-V-(*p*-Cl)$_2$ using a conventional procedure [25] and prepared iodide salts of the radical cations (*m*-MePy-V)I and [*m*-MePy-V-(*p*-Cl)$_2$]I using a reported procedure for salts with similar chemical structures [26]. For (*m*-MePy-V)$_2$Fe$_2$OCl$_6$, 1-butyl-3-methylimidazolium tetrachloroferrate (74 mg, 0.22 mmol) was slowly added to a solution of (*m*-MePy-V)I (100 mg, 0.22 mmol) in 300 ml of ethanol and stirred for 1 h. The black solid (*m*-MePy-V)$_2$Fe$_2$OCl$_6$ was then separated by filtration and recrystallized using acetone. For [*m*-MePy-V-(*p*-Cl)$_2$]$_2$Fe$_2$OCl$_6 \cdot$ (CH$_3$CN)$_2$, a solution of 1-butyl-3-methylimidazolium tetrachloroferrate (64 mg, 0.19 mmol) was slowly added to a solution of [*m*-MePy-V-(*p*-Cl)$_2$]I (100 mg, 0.19 mmol) in 300 ml of ethanol and stirred for 1 h. The black solid was then separated by filtration, and the recrystallization in acetonitrile yielded black crystals with a molecular formula of [*m*-MePy-V-(*p*-Cl)$_2$]$_2$Fe$_2$OCl$_6 \cdot$ (CH$_3$CN)$_2$.

X-ray intensity data were collected using a Rigaku AFC-8R Mercury CCD RA-Micro7 diffractometer with Mo-Kα radiation ($\lambda = 0.71075$ Å). The structure was determined via a direct method using SIR2004 [27] and was refined using the SHELXL97 crystal structure refinement program [28]. The structural refinement was carried out using anisotropic and isotropic thermal parameters for the nonhydrogen and hydrogen atoms, respectively. All the hydrogen atoms were placed at the calculated ideal positions. The magnetization was measured using a commercial SQUID magnetometer (MPMS-XL, Quantum Design). The experimental results were corrected for the diamagnetic contributions calculated by Pascal's method. The specific heat was measured using a commercial calorimeter (PPMS, Quantum Design) by using a thermal relaxation method. All the above experiments were performed using randomly oriented small single crystals.

Ab initio MO calculations were performed using the UB3LYP method as broken-symmetry hybrid density-functional theory calculations. All calculations were performed using the GAUSSIAN09 software package with the basis set 6-31G. The convergence criterion was set to 10^{-8} Hartree. To estimate the intermolecular exchange interaction of the molecular pairs, we employed a conventional evaluation scheme [29].

III. CRYSTAL STRUCTURE AND MAGNETIC MODEL

A. (*m*-MePy-V)$_2$Fe$_2$OCl$_6$

The crystallographic parameters of (*m*-MePy-V)$_2$Fe$_2$OCl$_6$ are summarized in Table I, and Fig. 1(a) shows its molecular structure. For the *m*-MePy-V molecule, the verdazyl ring (which includes four nitrogen atoms), two upper phenyl rings, and bottom pyridine ring are labeled R$_1$, R$_2$, R$_3$, and R$_4$, respectively. The dihedral angles R$_1$-R$_2$, R$_1$-R$_3$, and R$_1$-R$_4$ are approximately 18°, 19°, and 15°, respectively. The MO calculations indicate that approximately 58%, 19%, 17%, and

TABLE I. Crystallographic data for (*m*-MePy-V)$_2$Fe$_2$OCl$_6$ (salt **1**) and [*m*-MePy-V-(*p*-Cl)$_2$]$_2$Fe$_2$OCl$_6 \cdot$ (CH$_3$CN)$_2$ (salt **2**).

Sample	Salt **1**	Salt **2**
Formula	C$_{40}$H$_{38}$Cl$_6$Fe$_2$N$_{10}$O	C$_{44}$H$_{40}$Cl$_{10}$Fe$_2$N$_{12}$O
Crystal system	monoclinic	
Space group	$C2/c$	$P2_1/c$
Temperature	RT	
a/Å	27.422(5)	7.497(3)
b/Å	8.5394(16)	25.698(9)
c/Å	19.759(4)	13.764(5)
β/degrees	104.972(2)	95.690(5)
V/Å^3	4469.9(15)	2638.7(17)
Z	4	2
D_{calc}/g cm^{-3}	1.485	1.534
Total reflections	3647	4308
Reflection used	3202	3448
Parameters refined	268	315
R [$I > 2\sigma(I)$]	0.0535	0.0626
R_w [$I > 2\sigma(I)$]	0.1371	0.1687
Goodness of fit	1.075	1.066
CCDC	1919408	1919409

less than 6% of the total spin density is present on R$_1$, R$_2$, R$_3$, and R$_4$, respectively. This evaluated spin-density distribution is comparable to that of other verdazyl radicals. The Fe$_2$OCl$_6^{2-}$ anion has a bent structure with an Fe-O-Fe angle of ~150°, as shown in Fig. 1(b). The oxygen atom is located on a twofold rotation axis parallel to the *b* axis, and the geometry around the Fe atom is slightly distorted tetrahedral, as shown in Table II. The Fe-O distance is 1.75 Å, and the Fe-Cl bond distances are 2.18–2.22 Å. The obtained bond distances and angles are comparable to previously reported values [30].

We evaluated the intermolecular magnetic interactions using MO calculations. In the low-temperature region discussed in the present paper, the two $S = 5/2$ spins on the Fe$_2$OCl$_6^{2-}$ anion are considered to form a nonmagnetic singlet dimer through a strong AF interaction [30]. Thus, we calculated interactions only between *m*-MePy-V molecules based on crystallographic data. In the crystal, the *m*-MePy-V molecules are arranged two-dimensionally in the *bc* plane, and the Fe$_2$OCl$_6^{2-}$ anions are located between the 2D layers, as shown in Fig. 1(c). We determined two types of dominant interactions through MO calculations, evaluated as $J_a/k_B = 96.9$ K and $J_b/k_B = -6.4$ K; these are defined in the Heisenberg spin Hamiltonian given by $\mathcal{H} = J_n \sum_{\langle i,j \rangle} S_i \cdot S_j$, where $\sum_{\langle i,j \rangle}$ denotes the sum over neighboring spin pairs. The molecular pair related to J_a has an N-N short contact of 3.56 Å, which is related by inversion symmetry, as shown in Fig. 1(d). The molecular pair related to J_b has an N-C short contact of 3.32 Å, which is related by a twofold screw axis parallel to the *b* axis, as shown in Fig. 1(e). The two dominant interactions form an $S = 1/2$ honeycomb lattice in the *bc* plane, as shown in Fig. 1(f), in which the AF dimers formed by J_a are weakly connected by the ferromagnetic J_b.

B. [*m*-MePy-V-(*p*-Cl)$_2$]$_2$Fe$_2$OCl$_6 \cdot$ (CH$_3$CN)$_2$

The crystallographic parameters of [*m*-MePy-V-(*p*-Cl)$_2$]$_2$Fe$_2$OCl$_6 \cdot$ (CH$_3$CN)$_2$ are summarized in Table I,
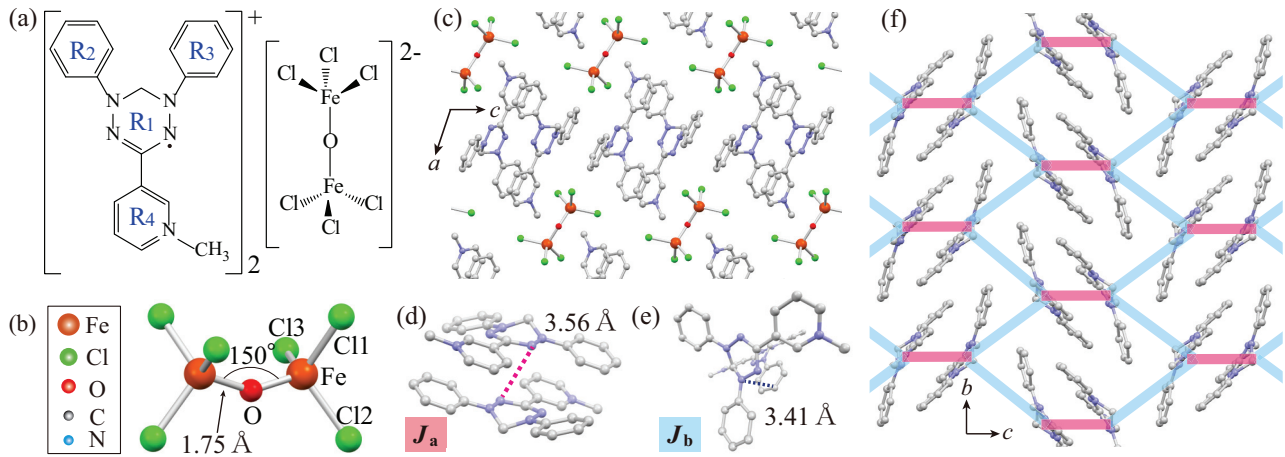
FIG. 1. (a) Molecular structure of $(m\text{-MePy-V})_2\text{Fe}_2\text{OCl}_6$. (b) $\text{Fe}_2\text{OCl}_6^{2-}$ anion forming a bent structure. (c) Crystal structure in the ac plane. Hydrogen atoms are omitted for clarity. Molecular pairs associated with exchange interactions (d) J_a and (e) J_b. The dashed lines indicate N-N and N-C short contacts. (f) Crystal structure of $(m\text{-MePy-V})_2\text{Fe}_2\text{OCl}_6$ in the bc plane. The lines represent J_a and J_b forming the honeycomb lattice.

and Fig. 2(a) shows its molecular structure. For the $m\text{-MePy-V-}(p\text{-Cl})_2$ molecule, verdazyl ring, two upper phenyl rings, and the bottom pyridine ring are labeled R_1, R_2, R_3, and R_4, respectively, and the dihedral angles $R_1\text{-}R_2$, $R_1\text{-}R_3$, and $R_1\text{-}R_4$ are approximately $21°$, $30°$, and $4°$, respectively. The MO calculations indicate that approximately 60%, 17%, 17%, and less than 6% of the total spin density is present on R_1, R_2, R_3, and R_4, respectively. The evaluated spin-density distribution is comparable to that of other verdazyl radicals. The $\text{Fe}_2\text{OCl}_6^{2-}$ anion has a linear structure with an Fe-O-Fe angle of $180°$ [31,32], as shown in Fig. 2(b), where the oxygen atom is located at the inversion center. The geometry around the Fe atom is slightly distorted tetrahedral, as shown in Table II ; the Fe-O bond distance is 1.74 Å, and the Fe-Cl bond distances are 2.21–2.22 Å. It was confirmed that there is no definitive structural difference between the two salts except for Fe-O-Fe angle.

We evaluated the intermolecular magnetic interactions using MO calculations. The two $S = 5/2$ spins on the $\text{Fe}_2\text{OCl}_6^{2-}$ anion in this salt are also considered to form a nonmagnetic singlet dimer through a strong AF intramolecular interaction below RT [30]. Thus, we calculated interactions only between $m\text{-MePy-V-}(p\text{-Cl})_2$ molecules based on crystallographic data. We determined four types of dominant interactions through the MO calculations evaluated as $J_1/k_B = 18.6\,\text{K}$, $J_2/k_B = 11.3\,\text{K}$, $J_3/k_B = -7.4\,\text{K}$, and $J_4/k_B = -2.5\,\text{K}$. The molecular pairs associated with J_1 and J_2 are related through their inversion center, and have C-C short contacts of 3.62 and 3.59 Å, respectively, as shown in Figs. 2(c) and 2(d). The molecular pairs associated with J_3 and J_4 have glide reflection symmetries, where the glide plane is parallel to the ac-plane, and have C-C short contacts of 3.53 and 3.63 Å, respectively, as shown in Figs. 2(e) and 2(f). Because J_3 and J_4 are caused by short contacts related to the R_4 ring with the lowest spin density, their absolute values are relatively small compared with the other interactions. In the crystal, the $m\text{-MePy-V-}(p\text{-Cl})_2$ molecules form a honeycomb-based 3D structure, where the $\text{Fe}_2\text{OCl}_6^{2-}$ anion and crystal solvent CH_3CN are located in the hexagonal structure, as shown in Fig. 2(g). Considering the evaluated intermolecular interactions, a honeycomb lattice is formed by J_1 and J_3 in the bc plane, which is connected three-dimensionally by J_2 and J_4, as shown in Figs. 2(g) and 2(h). Accordingly, an $S = 1/2$ honeycomb-based 3D spin model is formed, as shown in Fig. 3. One can consider this model as AF $J_1\text{-}J_2$ alternating chains connected by ferromagnetic J_3 and J_4.

TABLE II. Bond distances [Å] and angles [°] for $\text{Fe}_2\text{OCl}_6^{2-}$ anions in $(m\text{-MePy-V})_2\text{Fe}_2\text{OCl}_6$ (salt **1**) and $[m\text{-MePy-V-}(p\text{-Cl})_2]_2\text{Fe}_2\text{OCl}_6 \cdot (\text{CH}_3\text{CN})_2$ (salt **2**).

Salt **1**		Salt **2**	
Fe–O	1.75	Fe–O	1.74
Fe–Cl1	2.18	Fe–Cl1	2.22
Fe–Cl2	2.21	Fe–Cl2	2.21
Fe–Cl3	2.22	Fe–Cl3	2.22
Fe–O–Fe	149.5	Fe–O–Fe	180.0
O–Fe–Cl1	110.3	O–Fe–Cl1	112.4
O–Fe–Cl2	106.9	O–Fe–Cl2	111.6
O–Fe–Cl3	113.7	O–Fe–Cl3	109.6
Cl1–Fe–Cl2	109.5	Cl1–Fe–Cl2	107.8
Cl2–Fe–Cl3	107.6	Cl2–Fe–Cl3	109.2
Cl3–Fe–Cl1	108.8	Cl1–Fe–Cl1	106.1

IV. MAGNETIC AND THERMODYNAMIC PROPERTIES

A. $(m\text{-MePy-V})_2\text{Fe}_2\text{OCl}_6$

Figure 4 shows the temperature dependence of the magnetic susceptibility ($\chi = M/H$) of $(m\text{-MePy-V})_2\text{Fe}_2\text{OCl}_6$ at 0.5 T, showing a broad peak at approximately 50 K. The observed magnetic moment above this peak temperature indicates contributions from both $S = 1/2$ on the radical and $S = 5/2$ on the $\text{Fe}_2\text{OCl}_6^{2-}$ anion. Because the $S = 5/2$ spins on the $\text{Fe}_2\text{OCl}_6^{2-}$ anion are expected to form an AF dimer, we calculated the magnetic susceptibility of the Fe dimer and subtracted it from the raw data, as shown in Fig. 4(a).
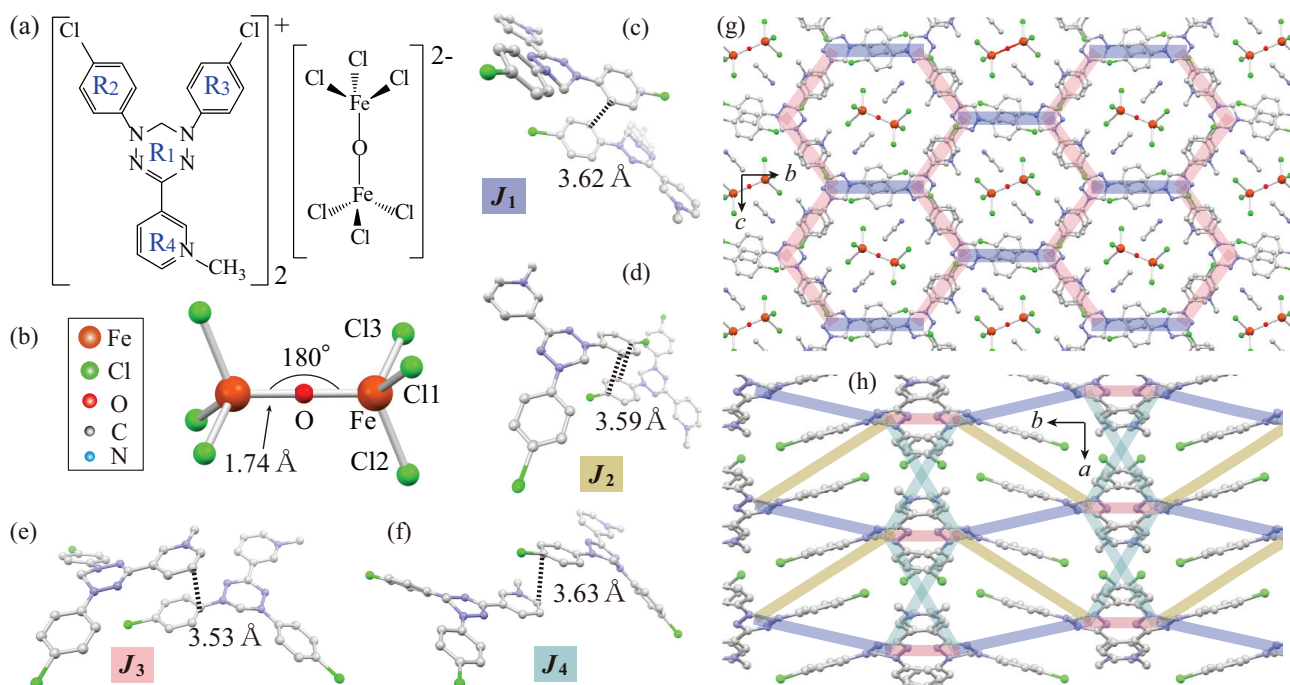
FIG. 2. (a) Molecular structure of [*m*-MePy-V-(*p*-Cl)$_2$]$_2$Fe$_2$OCl$_6$. (b) Fe$_2$OCl$_6^{2-}$ anion forming a linear structure. Molecular pairs associated with exchange interactions (c) J_1, (d) J_2, (e) J_3, and (f) J_4. The dashed lines indicate C-C short contacts. Crystal structure of [*m*-MePy-V-(*p*-Cl)$_2$]$_2$Fe$_2$OCl$_6 \cdot$ (CH$_3$CN)$_2$ in the (g) *bc* and (h) *ab* planes. Hydrogen atoms are omitted for clarity. The lines represent J_1, J_2, J_3, and J_4 forming the honeycomb-based 3D lattice.

Considering subsequent analysis of the radical contributions, we determined the Fe dimer interaction to be $J/k_B = 300(3)$ K, which is consistent with previously reported values [30]. This strong AF interaction forms a nonmagnetic singlet state, and its magnetic susceptibility exhibits an exponential decrease with decreasing temperature, as shown in Fig. 4(a). The subtracted data χ_v corresponds to the magnetic susceptibility of the $S = 1/2$ spins on the radical. We note that the upturn below $\sim$15 K is caused by slight paramagnetic impurities as-

FIG. 3. $S = 1/2$ honycomb-based 3D spin model composed of J_i ($i = 1$–4) in [*m*-MePy-V-(*p*-Cl)$_2$]$_2$Fe$_2$OCl$_6 \cdot$ (CH$_3$CN)$_2$.

sociated with lattice defects, which is commonly observed in verdazyl-based compounds [16,33,34]. Assuming the conventional paramagnetic behavior C_{imp}/T, where C_{imp} is the Curie constant of the impurities, we evaluated the paramagnetic impurities to be approximately 3.8 % of all spins and subtracted them from χ_v, as shown in Fig. 4(b). This corrected χ_v clearly exhibits an exponential decrease with decreasing temperature below the peak temperature, which is associated with the formation of an excitation gap. Additionally, considering the large distortion of the present honeycomb lattice, which corresponds to a dimerlike one [11,12], a gapped dimer phase is considered to occur. Thus, we calculated the magnetic susceptibility of the $S = 1/2$ AF dimer and obtained good agreement between the corrected χ_v and calculated results by using $J/k_B = 88(3)$ K, as shown in Fig. 4(b). The obtained interaction is confirmed to be close to that evaluated from the MO calculations.

The specific heat C_p at zero field indicates consistent behavior with the magnetic susceptibility, as shown in Fig. 5. There is no sharp peak associated with a phase transition to an ordered state. A Schottky-like peak associated with the energy gap is expected to appear at approximately 30 K. It is required to subtract a lattice contribution to discuss the magnetic specific heat. However, Debye's T^3 law for the lattice contribution is confirmed to be applicable only below approximately 10 K in verdazyl radical compounds [16,21,33]. Accordingly, the evaluation of the lattice contribution is difficult in the temperature regions discussed here, and the expected Schottky-like peak is masked by the lattice contributions.
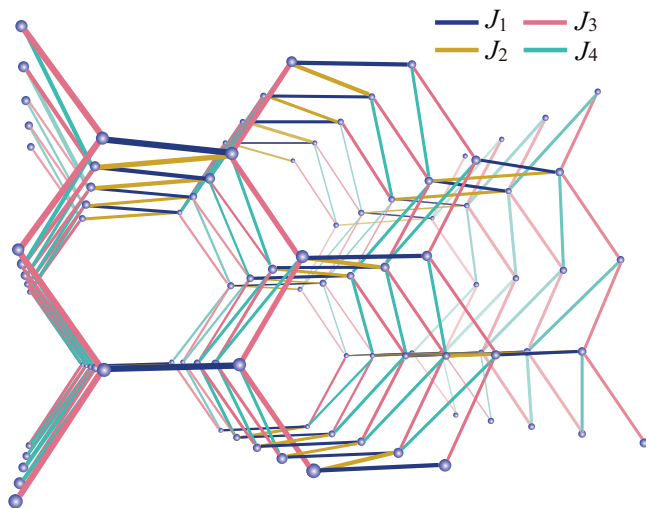
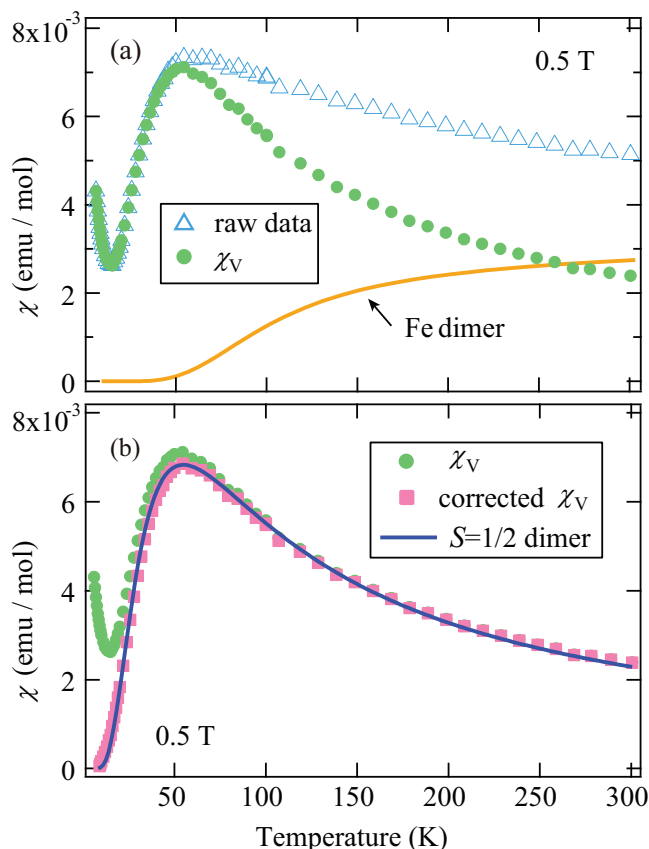FIG. 5. Temperature dependence of specific heat C_p of $(m\text{-MePy-V})_2\text{Fe}_2\text{OCl}_6$.

FIG. 4. Temperature dependence of magnetic susceptibility ($\chi = M/H$) of $(m\text{-MePy-V})_2\text{Fe}_2\text{OCl}_6$ at 0.5 T. The solid lines in (a) and (b) represent the calculated results for the $S = 5/2$ Fe dimer and $S = 1/2$ dimer coupled by J_1. The open triangles denote raw data, and χ_v shows the contribution of $S = 1/2$ spins on the radical, which is obtained by subtracting the Fe dimer from the raw data. The corrected χ_v is adjusted to account for the paramagnetic term due to impurities.

B. [m-MePy-V-(p-Cl)$_2$]$_2$Fe$_2$OCl$_6$ · (CH$_3$CN)$_2$

Figure 6 shows the temperature dependence of the magnetic susceptibility ($\chi = M/H$) of [m-MePy-V -(p-Cl)$_2$]$_2$Fe$_2$OCl$_6$ · (CH$_3$CN)$_2$ at 0.05 T, showing a broad peak at approximately 18 K. The values of χT above this peak temperature indicate contributions from both $S = 1/2$ on the radical and $S = 5/2$ on the Fe$_2$OCl$_6$ anion, as shown in the inset of Fig. 6. Because the $S = 5/2$ spins on the Fe$_2$OCl$_6^{2-}$ anion are likewise expected to form an AF dimer, we calculated the magnetic susceptibility of the Fe dimer and subtracted it from the raw data. The Fe dimer interaction was determined to become almost $\chi T = 0.75$, which is the expected value for noninteracting $S = 1/2$ spins, in the high-temperature region, as shown in the inset of Fig. 6. Thus, we obtained $J/k_B = 302(3)$ K, which is very close to that of $(m\text{-MePy-V})_2\text{Fe}_2\text{OCl}_6$. The nearly equivalent Fe dimer interactions in the two salts suggest that the strength of the exchange interaction in Fe$_2$OCl$_6^{2-}$ is almost independent of the Fe-O-Fe angle. The subtracted data χ_v corresponds to the magnetic susceptibility of $S = 1/2$ spins on the radical and can be considered to arise from the $S = 1/2$
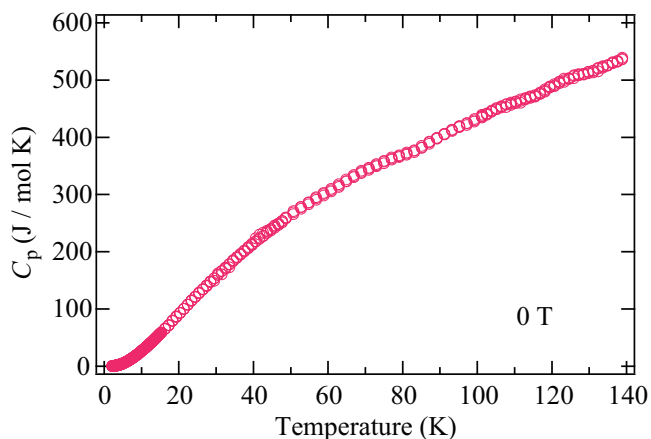
honeycomb-based 3D spin model. In the low-temperature region, $\chi_v T$ decreases with decreasing temperature, indicating dominant contributions of AF interactions. Furthermore, we observed a discontinuous change at approximately 5 K, which is considered to be associated with a phase transition to an AF 3D long-range order (LRO). The upturn in the lower temperature region is considered to arise from slight paramagnetic impurities and/or a small magnetic anisotropy accompanied by the LRO [35].

Figure 7 shows the temperature dependence of the specific heat C_p at zero field. We found an anomaly at 4.8 K, which is consistent with the discontinuous change in the magnetic
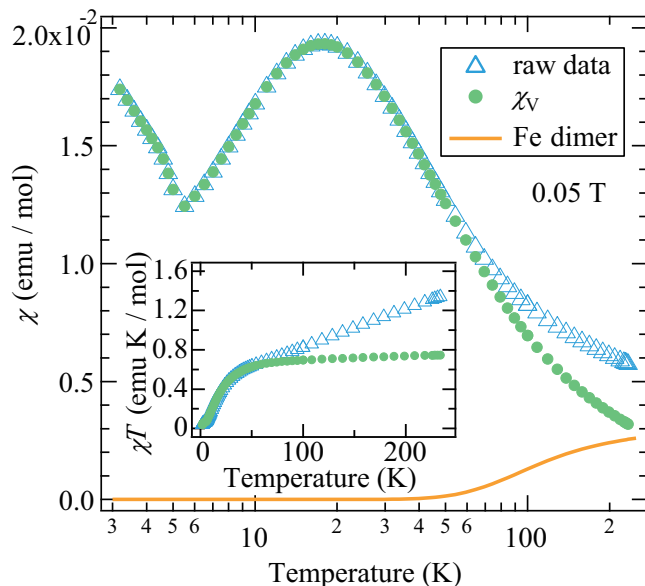

FIG. 6. Temperature dependence of magnetic susceptibility ($\chi = M/H$) of [m-MePy-V-(p-Cl)$_2$]$_2$Fe$_2$OCl$_6$ · (CH$_3$CN)$_2$ at 0.05 T. The solid line represents the calculated result for the $S = 5/2$ Fe dimer. The open triangles denote raw data and χ_v shows the contribution of $S = 1/2$ spins on the radical, which was obtained by subtracting the Fe dimer from the raw data. The inset shows the temperature dependence of χT.
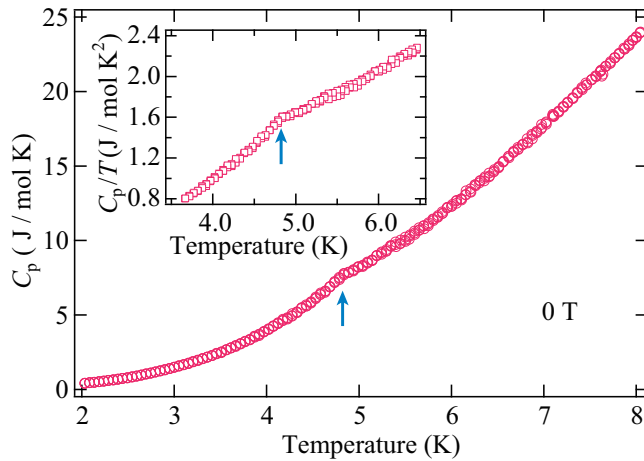
FIG. 7. Temperature dependence of specific heat C_p of $[m\text{-MePy-V-}(p\text{-Cl})_2]_2\text{Fe}_2\text{OCl}_6 \cdot (\text{CH}_3\text{CN})_2$. The inset shows the temperature dependence of C_p/T. The arrows indicate the phase-transition temperature.

susceptibility and is direct evidence for the phase transition to the 3D LRO. Since divergent behavior was not observed at the phase transition, there must exist sufficient development of a short-range order in the dominant AF J_1-J_2 chain accompanied by a large entropy loss, resulting in the small anomaly at the phase transition.

V. SUMMARY

We have succeeded in synthesizing single crystals of the verdazyl-based salts $(m\text{-MePy-V})_2\text{Fe}_2\text{OCl}_6$ and $m\text{-MePy-V-}(p\text{-Cl})_2]_2\text{Fe}_2\text{OCl}_6 \cdot (\text{CH}_3\text{CN})_2$ with different Fe_2OCl_6 structures. These salts demonstrated the formation of different types of $S = 1/2$ honeycomb-based lattices in the low-temperature region. For the former salt, the $\text{Fe}_2\text{OCl}_6^{2-}$ anion has a bent structure with an Fe-O-Fe angle of $150°$, and the AF interaction between $S = 5/2$ spins of the Fe^{3+} ions was

evaluated to be 300(3) K from the magnetization analysis. The nearly equivalent exchange interactions between Fe^{3+} ions in the two salts suggest that the Fe-O-Fe angle has little influence on the strength of the exchange interaction. We subtracted the contribution of the $S = 5/2$ spins from the observed magnetic susceptibility and considered the subtracted data as the magnetic susceptibility of the radical $S = 1/2$ spins. The MO calculations indicated that $S = 1/2$ AF dimers through J_a are weakly connected by ferromagnetic interactions J_b, thereby forming a honeycomb lattice. The magnetic susceptibility and specific heat indicated a nonmagnetic gapped behavior, and the magnetic behavior was explained using a dominant $S = 1/2$ AF dimer model coupled by J_a. For the latter salt, the $\text{Fe}_2\text{OCl}_6^{2-}$ anion has a linear structure with an Fe-O-Fe angle of $180°$, and the corresponding exchange interaction was evaluated to be 302(3) K from magnetization analysis. The contribution of $S = 1/2$ spins on the radical to the magnetic susceptibility was also evaluated by subtracting the contribution of the $S = 5/2$ spins. MO calculations indicated that four types of dominant interactions form an unconventional $S = 1/2$ honeycomb-based 3D spin model. The magnetic susceptibility and specific heat indicated a phase transition to a 3D LRO at approximately 4.8 K. The present work demonstrates that verdazyl-based salt can form a variety of $S = 1/2$ HAF honeycomb lattices with a dimerlike distortion. The modulation of the exchange interactions through our molecular design have the potential to produce similar spin models with smaller energy gaps, which will provide an opportunity to investigate transport properties in a magnon BEC on a honeycomb lattice. Further, it will stimulate theoretical studies on honeycomb-based quantum spin systems.

[1] K. S. Novoselov, A. K. Geim, S. V. Morozov, D. Jiang, M. I. Katsnelson, I. V. Grigorieva, S. V. Dubonos, and A. Firsov, Nature **438**, 197 (2005).

[2] X. Du, I. Skachko, F. Duerr, A. Luican, and E. Y. Andrei, Nature **462**, 192 (2009).

[3] A. H. Castro Neto, F. Guinea, N. M. R. Peres, K. S. Novoselov, and A. K. Geim, Rev. Mod. Phys. **81**, 109 (2009).

[4] A. Kitaev, Ann. Phys. (NY) **321**, 2 (2006).

[5] G. Baskaran, S. Mandal, and R. Shankar, Phys. Rev. Lett. **98**, 247201 (2007).

[6] G. Jackeli and G. Khaliullin, Phys. Rev. Lett. **102**, 17205 (2009).

[7] Z. Weihong, J. Oitmaa, and C. J. Hamer, Phys. Rev. B **44**, 11869 (1991).

[8] J. Oitmaa, C. J. Hamer, and Zheng Weihong, Phys. Rev. B **45**, 9834 (1992).

[9] E. V. Castro, N. M. R. Peres, K. S. D. Beach, and A. W. Sandvik, Phys. Rev. B **73**, 054422 (2006).

[10] H. C. Jiang, Z. Y. Weng, and T. Xiang, Phys. Rev. Lett. **101**, 090603 (2008).

[11] K. Takano, Phys. Rev. B **74**, 140402(R) (2006).

[12] W. Li, S.-S. Gong, Y. Zhao, and G. Su, Phys. Rev. B **81**, 184427 (2010).

[13] V. Kataev, A. Möller, U. Löw, W. Jung, N. Schittner, M. Kriener, and A. Freimuth, J. Magn. Magn. Mater. **290–291**, 310 (2005).

[14] A. A. Tsirlin, O. Janson, and H. Rosner, Phys. Rev. B **82**, 144416 (2010).

[15] Z. Honda, T. Kodama, R. Kikukawa, M. Hagiwara, T. Kida, M. Sakai, T. Fukuda, T. Fujihara, and N. Kamata, J. Phys. Soc. Jpn. **84**, 034601 (2015).

[16] H. Yamaguchi, K. Iwase, T. Ono, T. Shimokawa, H. Nakano, Y. Shimura, N. Kase, S. Kittaka, T. Sakakibara, T. Kawakami, and Y. Hosokoshi, Phys. Rev. Lett. **110**, 157205 (2013).

[17] H. Yamaguchi, H. Miyagai, T. Shimokawa, K. Iwase, T. Ono, Y. Kono, N. Kase, K. Araki, S. Kittaka, T. Sakakibara, T. Kawakami, K. Okunishi, and Y. Hosokoshi, J. Phys. Soc. Jpn. **83**, 033707 (2014).

[18] H. Yamaguchi, T. Okubo, K. Iwase, T. Ono, Y. Kono, S. Kittaka, T. Sakakibara, A. Matsuo, K. Kindo, and Y. Hosokoshi, Phys. Rev. B **88**, 174410 (2013).

[19] H. Yamaguchi, T. Okubo, S. Kittaka, T. Sakakibara, K. Araki, K. Iwase, N. Amaya, T. Ono, and Y. Hosokoshi, Sci. Rep. **5**, 15327 (2015).

[20] H. Yamaguchi, M. Okada, Y. Kono, S. Kittaka, T. Sakakibara, T. Okabe, Y. Iwasaki, and Y. Hosokoshi, Sci. Rep. **7**, 16144 (2017).

[21] H. Yamaguchi, A. Toho, K. Iwase, T. Ono, T. Kawakami, T. Shimokawa, A. Matsuo, and Y. Hosokoshi, J. Phys. Soc. Jpn. **82**, 043713 (2013).

[22] T. Okabe, H. Yamaguchi, S. Kittaka, T. Sakakibara, T. Ono, and Y. Hosokoshi, Phys. Rev. B **95**, 075120 (2017).

[23] H. Yamaguchi, Y. Tamekuni, Y. Iwasaki, and Y. Hosokoshi, Phys. Rev. B **97**, 201109(R) (2018).

[24] H. Yamaguchi, Y. Sasaki, T. Okubo, M. Yoshida, T. Kida, M. Hagiwara, Y. Kono, S. Kittaka, T. Sakakibara, M. Takigawa, Y. Iwasaki, and Y. Hosokoshi, Phys. Rev. B **98**, 094402 (2018).

[25] R. Kuhn, Angew. Chem. **76**, 691 (1964).

[26] K. Mukai, S. Jinno, Y. Shimobe, N. Azuma, M. Taniguchi, Y. Misaki, K. Tanaka, K. Inoue, and Y. Hosokoshi, J. Mater. Chem. **13**, 1614 (2003).

[27] M. C. Burla, R. Caliandro, M. Camalli, B. Carrozzini, G. L. Cascarano, L. De Caro, C. Giacovazzo, G. Polidori, and R. Spagna, J. Appl. Crystallogr. **38**, 381 (2005).

[28] G. M. Sheldrick, SHELXL97, program for crystal structure determination, University of Göttingen, Germany, 1997.

[29] M. Shoji, K. Koizumi, Y. Kitagawa, T. Kawakami, S. Yamanaka, M. Okumura, and K. Yamaguchi, Chem. Phys. Lett. **432**, 343 (2006).

[30] G. Haselhorst, K. Wieghardt, S. Keller, and B. Schrader, Inorg. Chem. **32**, 520 (1993).

[31] A. Lledós, M. Moreno-Mañas, M. Sodupe, A. Vallribera, I. Mata, B. Martínez, and E. Molins, Eur. J. Inorg. Chem. **2003**, 4187 (2003).

[32] T. Koike, S. Yokota, H. Fujiwara, T. Sugimoto, S. Noguchi, D. de Caro, and L. Valade, Inorg. Chem. **47**, 7074 (2008).

[33] H. Yamaguchi, Y. Shinpuku, T. Shimokawa, K. Iwase, T. Ono, Y. Kono, S. Kittaka, T. Sakakibara, and Y. Hosokoshi, Phys. Rev. B **91**, 085117 (2015).

[34] Y. Iwasaki, Y. Sasaki, Y. Hosokoshi, A. Matsuo, K. Kindo, and H. Yamaguchi, J. Phys. Soc. Jpn. **88**, 044709 (2019).

[35] H. Yamaguchi, Y. Tamekuni, Y. Iwasaki, R. Otsuka, Y. Hosokoshi, T. Kida, and M. Hagiwara, Phys. Rev. B **95**, 235135 (2017).